

Architecture and Dynamics of C<sub>22</sub> Bonded InterphasesMatthias Pursch,<sup>†,‡</sup> Lane C. Sander,<sup>‡</sup> Hans-J. Egelhaaf,<sup>§</sup> Martin Raitza,<sup>†</sup> Stephen A. Wise,<sup>‡</sup> Dieter Oelkrug,<sup>§</sup> and Klaus Albert<sup>\*,†</sup>

Contribution from the Institut für Organische Chemie der Universität Tübingen, Auf der Morgenstelle 18, and Institut für Physikalische und Theoretische Chemie der Universität Tübingen, Auf der Morgenstelle 8, D-72076 Tübingen, Germany, and National Institute of Standards and Technology (NIST), Gaithersburg, Maryland 20899

Received August 24, 1998. Revised Manuscript Received February 5, 1999

**Abstract:** The relationship between alkyl phase structure and chromatographic performance is investigated for a series of docosyl (C<sub>22</sub>)-modified silica surfaces. The results of solid-state nuclear magnetic resonance (NMR) spectroscopy and fluorescence spectroscopy are evaluated and correlated with liquid chromatographic retention for relevant shape-selective separations. A set of four different stationary phases was prepared by solution and surface polymerization approaches, yielding materials with surface coverages ranging from 3.6 to 7.0 μmol/m<sup>2</sup>. <sup>13</sup>C cross polarization magic angle spinning (CP/MAS) NMR spectra indicate that a predominance of trans conformations exists for high-coverage C<sub>22</sub> phases (>4.0 μmol/m<sup>2</sup>). Two-dimensional solid-state NMR spectroscopy (wide line separation, WISE) was utilized to evaluate the mobility of the trans and gauche alkyl chain conformations. Temperature-dependent <sup>13</sup>C CP/MAS NMR measurements of the bonded phases exhibit large differences in the dynamic behavior of the immobilized C<sub>22</sub> chains. Unusually high chain rigidity was found for the self-assembled monolayer C<sub>22</sub> phase (7.0 μmol/m<sup>2</sup>). Fluorescence lifetime measurements of 1,6-diphenylhexatriene (DPH) exhibit two different lifetimes of τ<sub>F</sub> ≈ 1 and 7 ns, which are ascribed to probe molecule populations in the mobile and bonded phases, respectively. Quantitative evaluation of the fluorescence decay curves shows that the partitioning of DPH into the alkyl phase is favored at higher surface coverages, reaching a maximum at a ligand density of 4.9 μmol/m<sup>2</sup>. Time-resolved fluorescence anisotropy measurements also revealed that probe mobility was minimized at this surface coverage. With increasing temperature, the mobility of DPH was found to increase and the fraction of sorbed molecules to decrease. A shape selectivity test mixture containing five polycyclic aromatic hydrocarbons including DPH was employed for temperature-dependent chromatographic studies. In accord with the spectroscopic results, shape selectivity is enhanced at low temperatures and at high surface coverages. The combination of these spectroscopic and chromatographic tools provides a wealth of information on the surface morphology of systematically prepared C<sub>22</sub> sorbents and greater insight on the molecular recognition process in liquid chromatography.

## Introduction

Alkyl stationary phases are widely used as separations media in liquid chromatography (LC). Most of these applications utilize monomeric bonded phases operated in the reversed-phase (RP) mode (i.e., using a relatively polar mobile-phase solvent). These materials are obtained by covalent surface reaction of a monofunctional silane with silica gel.<sup>1</sup> Polymeric bonded phases<sup>2</sup> (prepared with di- or trifunctional silanes in the presence of water) offer increased selectivity for rigid solutes compared to that of monomeric phases<sup>3</sup> and are commonly used for the separation of polycyclic aromatic hydrocarbons (PAHs)<sup>4–7</sup> and

carotenoids.<sup>8</sup> An understanding of the polymerization reaction and the study of the complex architecture of polymeric bonded phases remain a challenge. However, this knowledge is requisite to an understanding of molecular recognition processes in LC that will facilitate method development and enable the development of new selective and efficient RP materials.

In recent years, self-assembled monolayer (SAM) technology has received considerable attention.<sup>9,10</sup> Recent papers have presented studies of the surface properties of (mostly C<sub>18</sub>) alkylthiols on gold nanoparticles<sup>11–14</sup> and C<sub>18</sub> ligands on

<sup>†</sup> Institut für Organische Chemie der Universität Tübingen.

<sup>§</sup> Institut für Physikalische und Theoretische Chemie der Universität Tübingen

<sup>‡</sup> National Institute of Standards and Technology.

(1) Unger, K. K. *Packings and Stationary Phases in Chromatographic Techniques*; Marcel Dekker: New York, 1998.

(2) Sander, L. C.; Wise, S. A. *Anal. Chem.* **1984**, *56*, 504–510.

(3) Wise, S. A.; Sander, L. C. In *Chromatographic Separations Based on Molecular Recognition*; Jinno, K., Ed.; Wiley-VCH: New York, 1997; pp 1–64.

(4) Wise, S. A.; Bonnett, W. J.; Guenther, F. R.; May, W. E. *J. Chromatogr. Sci.* **1981**, *19*, 457–465.

(5) Sander, L. C.; Wise, S. A. In *Retention and Selectivity Studies in HPLC*; Smith, R. M., Ed.; Elsevier: Amsterdam, 1994; pp 337–369.

(6) Wise, S. A.; Sander, L. C.; May, W. E. *J. Chromatogr. A* **1993**, *642*, 329–349.

(7) Poster, D. L.; Sander, L. C.; Wise, S. A. In *The Handbook of Environmental Chemistry: Volume 3. Anthropogenic Compounds*; Hutzinger, O., Ed.; Springer-Verlag: Berlin, 1998; pp 77–135.

(8) Sander, L. C.; Sharpless, K. E.; Craft, N. E.; Wise, S. A. *Anal. Chem.* **1994**, *66*, 1667–1674.

(9) Dubois, L. H.; Nuzzo, R. G. *Annu. Rev. Phys. Chem.* **1992**, *43*, 437–463.

(10) Ulman, A. *Chem. Rev.* **1996**, *96*, 1533–1554.

(11) Badia, A.; Singh, S.; Demers, L.; Cuccia, L.; Brown, G. R.; Lennox, R. B. *Chem. Eur. J.* **1996**, *2*, 359–363.

(12) Badia, A.; Gao, W.; Singh, S.; Demers, L.; Cuccia, L.; Reven, L. *Langmuir* **1996**, *12*, 1262–1269.

(13) Badia, A.; Cuccia, L.; Demers, L.; Morin, F.; Lennox, R. B. *J. Am. Chem. Soc.* **1997**, *119*, 2682–2692.

nonporous silica<sup>15</sup> and zirconia.<sup>16</sup> These studies concluded that the alkyl chains are predominantly in trans conformations, suggesting a very high degree of order and density due to the self-assembly. Early work with SAMs of alkyl silanes on silicon substrates was performed by Maoz and Sagiv<sup>17</sup> and Wasserman et al.,<sup>18</sup> with characterization of these materials via ellipsometry, X-ray reflection, and infrared (IR) spectroscopy. Wirth and co-workers adopted the SAM concept for preparation of mixed C<sub>3</sub>/C<sub>18</sub><sup>19–21</sup> and C<sub>1</sub>/C<sub>18</sub><sup>22</sup> bonded phases. These materials, termed “horizontally polymerized phases”, have been shown to be well suited for chromatographic separations of charged compounds such as biomolecules, due to a reduction of accessible silanol sites on the silica.<sup>23</sup> Sander and Wise described the preparation of homogeneous C<sub>18</sub> SAM phases (surface polymerization).<sup>24,25</sup> They noted an increase in surface coverage compared to that obtained with conventional polymeric synthesis (solution polymerization) and suggested that more regular alkyl chain spacing results from the surface polymerization approach. Solid-state NMR investigations of both stationary phase types confirmed that alkyl chain spacing is more regular for surface-polymerized phases.<sup>26</sup>

A number of efforts have been made to describe the chromatographic properties of these materials. Wise et al. observed that the liquid chromatographic retention of PAHs is related to solute shape.<sup>4</sup> They defined a molecular descriptor known as “length-to-breadth” (L/B) ratio by a box drawn to enclose the molecule and demonstrated that solute retention for PAH isomers was correlated with this descriptor, especially for polymeric C<sub>18</sub> stationary phases. Thus, long, narrow solutes are retained longer than square-shaped solutes among isomer sets. An empirical model was later developed termed the “slot model”,<sup>27</sup> which described solute retention in terms of penetration into the space between alkyl chains (“slots”). Bulky, square, or nonplanar molecules would be excluded and have less retention than extended, planar molecules.

Several research groups have searched for a rigorous mathematical theory to describe solute retention in RPLC on alkyl stationary phases. Early efforts of Horvath et al.<sup>28,29</sup> and Karger et al.,<sup>30</sup> sometimes referred to as “hydrophobic or solvophobic retention theory”, utilized thermodynamic approaches to relate retention to the energetics of cavity formation within the mobile

and stationary phases. These theories were consistent with overall retention trends observed for polar and nonpolar solutes, but the theory failed to adequately explain retention differences resulting from differences in stationary phase bonding chemistry or solute shape. Yan and Martire utilized a statistical mechanical “lattice model” approach to describe retention processes.<sup>31,32</sup> A similar approach has also been published by Dill.<sup>33</sup> Unlike previous efforts, these interphase models predict that conformational order of the immobilized alkyl chains will directly influence solute interactions and, consequently, solute retention. Thus, an understanding of stationary phase morphology is requisite to understanding solute retention processes.

A number of approaches have been used in the study and characterization of alkyl-modified surfaces, including IR<sup>19,34</sup> and Raman spectroscopy,<sup>35</sup> photoacoustic spectroscopy,<sup>36</sup> small-angle neutron scattering (SANS),<sup>37</sup> and molecular modeling.<sup>38</sup>

Solid-state NMR spectroscopy is one of the most powerful tools for studying the surface morphology of alkyl stationary phases. NMR experiments can be designed to probe conformational structure and dynamic aspects as well as bonding chemistry of immobilized alkyl ligands through observation of <sup>1</sup>H, <sup>13</sup>C, and <sup>29</sup>Si nuclei present in the interphases. The combination of cross polarization (CP)<sup>39,40</sup> with magic angle spinning (MAS)<sup>41</sup> allows acquisition of high-resolution NMR spectra of low-abundance heteronuclei (e.g., <sup>13</sup>C and <sup>29</sup>Si) in reasonable measuring times,<sup>42</sup> and a number of CP/MAS NMR investigations of bonded phases have been reported.<sup>43–46</sup> Since high-speed MAS NMR probes are available, the utilization of <sup>1</sup>H MAS NMR spectroscopy with spinning speeds of 14 000 Hz and higher provides a rapid method for characterization of structure and mobility of bonded phases.<sup>47</sup> Recently, multidimensional solid-state NMR methods have been developed to study inhomogeneities and mobilities of organic polymers.<sup>48</sup> The so-called two-dimensional wide line separation (2D WISE) experiment<sup>49,50</sup> combines the information on structure (<sup>13</sup>C chemical shifts) with segmental mobility (<sup>1</sup>H line widths). This experiment is of considerable interest for the study of dynamics of different alkyl chain conformations.

(14) Berger, R.; Delamarche, E.; Lang, H. P.; Gerber, C.; Gimzewski, J. K.; Meyer, E.; Güntherodt, H. *J. Science* **1997**, *276*, 2021–2024.

(15) Gao, W.; Reven, L. *Langmuir* **1995**, *11*, 1860–1863.

(16) Gao, W.; Dickinson, L.; Grozinger, C.; Morin, F. G.; Reven, L. *Langmuir* **1997**, *13*, 115–118.

(17) Maoz, R.; Sagiv, J. *Langmuir* **1987**, *3*, 1034–1044.

(18) Wasserman, S. R.; Whitesides, G. M.; Tidswell, I. M.; Ocko, B. M.; Pershan, P. S.; Axe, J. D. *J. Am. Chem. Soc.* **1989**, *111*, 5852–5861.

(19) Wirth, M. J.; Fatunmbi, H. O. *Anal. Chem.* **1992**, *64*, 2783–2788.

(20) Wirth, M. J.; Fatunmbi, H. O. *Anal. Chem.* **1993**, *65*, 822–826.

(21) Fatunmbi, H. O.; Bruch, M. D.; Wirth, M. J. *Anal. Chem.* **1993**, *65*, 2048–2054.

(22) Fairbank, R. W. P.; Xiang, Y.; Wirth, M. J. *Anal. Chem.* **1995**, *67*, 3879–3885.

(23) Wirth, M. J.; Fairbank, R. W. P.; Fatunmbi, H. O. *Science* **1997**, *275*, 44–47.

(24) Sander, L. C.; Wise, S. A. *Anal. Chem.* **1995**, *67*, 3284–3292.

(25) Sander, L. C.; Wise, S. A. In *Advances in Chromatography*; Giddings, J. C., Grushka, E., Cazes, J., Brown, P. R., Eds.; Marcel Dekker: New York, 1986; pp 139–218.

(26) Pursch, M.; Sander, L. C.; Albert, K. *Anal. Chem.* **1996**, *68*, 4107–4113.

(27) Wise, S. A.; Sander, L. C. *J. High Resolut. Chromatogr. Chromatogr. Commun.* **1985**, *8*, 248–255.

(28) Horvath, Cs.; Melander, W. R.; Molnar, I. J. *Chromatogr.* **1976**, *125*, 129–156.

(29) Horvath, Cs.; Melander, W. R. *J. Chromatogr. Sci.* **1977**, *15*, 393–404.

(30) Karger, B. L.; Gant, J. R.; Hartkopf, A.; Weiner, P. H. *J. Chromatogr.* **1976**, *128*, 65–78.

(31) Yan, C.; Martire, D. E. *J. Phys. Chem.* **1992**, *96*, 3489–3504.

(32) Yan, C.; Martire, D. E. *Anal. Chem.* **1992**, *64*, 1246–1253.

(33) Dill, K. A. *J. Phys. Chem.* **1987**, *91*, 1980–1988.

(34) Sander, L. C.; Callis, J. B.; Field, L. R. *Anal. Chem.* **1983**, *55*, 1068–1075.

(35) Ho, M.; Cai, M.; Pemberton, J. E. *Anal. Chem.* **1997**, *69*, 2613–2616.

(36) Lochmüller, C. H.; Marshall, S. F.; Wilder, D. R. *Anal. Chem.* **1980**, *52*, 19–23.

(37) Sander, L. C.; Glinka, C. J.; Wise, S. A. *Anal. Chem.* **1990**, *62*, 1099–1101.

(38) Yarowski, I.; Aguilar, M.; Hearn, M. T. W. *Anal. Chem.* **1995**, *67*, 2145–2153.

(39) Hartmann, S. R.; Hahn, E. L. *Phys. Rev.* **1962**, *128*, 2042.

(40) Pines, A.; Gibby, M. G.; Waugh, J. S. *J. Chem. Phys.* **1972**, *56*, 1776.

(41) Andrew, E. R.; Bradbury, A.; Eades, R. G. *Nature* **1959**, *183*, 1802.

(42) Schaefer, J.; Stejskal, E. O. *J. Am. Chem. Soc.* **1976**, *98*, 1031–1032.

(43) Maciel, G. E.; Sindorf, D. W. *J. Am. Chem. Soc.* **1980**, *102*, 7606–7607.

(44) Sindorf, D. W.; Maciel, G. E. *J. Am. Chem. Soc.* **1983**, *105*, 1848–1851.

(45) Bayer, E.; Albert, K.; Reiners, J.; Nieder, M.; Müller, D. *J. Chromatogr.* **1983**, *264*, 197–213.

(46) Albert, K.; Bayer, E. *J. Chromatogr.* **1991**, *544*, 345–370.

(47) Brindle, R.; Pursch, M.; Albert, K. *Solid State Nucl. Magn. Reson.* **1996**, *6*, 251–265.

(48) Schmidt-Rohr, K.; Spiess, H. W. *Multidimensional Solid-State NMR and Polymers*; Academic Press: London, 1994.

(49) Schmidt-Rohr, K.; Clauss, J.; Spiess, H. W. *Macromolecules* **1992**, *25*, 5, 3273–3277.

(50) Clauss, J.; Schmidt-Rohr, K.; Adam, A.; Boeffel, C.; Spiess, H. W. *Macromolecules* **1992**, *25*, 5208–5214.

**Table 1.** Reaction Conditions and Properties of C<sub>22</sub> Bonded Phases

phase	polymerization type	silane functionality	conditions	% C	coverage ( $\mu\text{mol}/\text{m}^2$ )	$\alpha_{\text{TBN/BaP}}^a$	comments
<b>A</b>	solution	dichloro	reflux	15.01	3.61	1.25	1.0 mL of H <sub>2</sub> O added
<b>B</b>	surface	dichloro	ambient	18.33	4.65	0.70	humidified silica
<b>C</b>	solution	trichloro	reflux	18.17	4.89	0.47	1.0 mL of H <sub>2</sub> O added
<b>D</b>	surface	trichloro	ambient	23.38	6.97	0.12	humidified silica

<sup>a</sup> See text.

Fluorescence spectroscopy<sup>51–53</sup> has proven to be a valuable method for determining the microenvironment and mobility of solutes in organic interphases such as polystyrene/poly(ethylene glycol) microbeads<sup>53</sup> and chromatographic bonded phases.<sup>54</sup> The polarity and microviscosity of bonded phases have been measured with fluorescent probes to elucidate the dependence of structure and dynamics of these phases on ligand density, alkyl chain length, temperature, and liquid phase composition. The polarity of the interphase, determined mainly by the amount of solvent associated with it, has been obtained from the peak ratio of pyrene fluorescence spectra<sup>55–58</sup> or from the Stokes shift of dansyl moieties.<sup>59</sup> It was found that the amount of sorbed solvent decreases with the polarity of the solvent<sup>56–58</sup> and with increasing chain length.<sup>60</sup> Solvent sorption is also reduced in highly ordered phases, e.g., in polymeric phases and on planar surfaces, as indicated by total internal reflection fluorescence (TIRF) experiments.<sup>61</sup> The protection of sorbed probe molecules from the mobile phase depends on liquid phase composition<sup>55,58,62</sup> and on alkyl chain length,<sup>62</sup> as revealed by fluorescence quenching studies. In most cases, several populations of sorbed fluorescent probe molecules exist. Nonpolar molecules such as pyrene and 1,6-diphenylhexatriene (DPH) are preferentially located in less polar regions more remote from the surface,<sup>55</sup> which makes them less accessible to quenchers.<sup>55</sup> In the presence of water, the alkyl chains collapse onto the surface,<sup>56,57,62</sup> thereby trapping nonpolar probe molecules and effectively protecting them from the solvent. Trapped pyrene probes indicate that the polarity of this environment corresponds to that of 1-octanol.<sup>56</sup>

The microviscosity of bonded phases has been determined by pyrene excimer formation,<sup>63,64</sup> rendering a value of  $\eta = 0.018$  Pa·s for the microviscosity of a C<sub>18</sub> phase in a methanol/water mixture.<sup>63</sup> The same value was obtained by time-resolved fluorescence anisotropy measurements of DPH on C<sub>18</sub> alkyl bonded planar silica surfaces using the TIRF technique.<sup>65</sup> TIRF anisotropy techniques have also been used to determine order

and orientation of the bonded alkyl chains from the orientation of sorbed solute.<sup>66</sup>

In our studies to better understand the influence of alkyl chain conformational order of RP materials on their separation behavior in liquid chromatography (LC), we have investigated the morphology of C<sub>18</sub><sup>26</sup> and C<sub>30</sub><sup>67</sup> bonded phases. This paper presents the application and correlation of three independent analytical and spectroscopic methods (solid-state NMR spectroscopy, fluorescence spectroscopy, and LC) for the study of shape selectivity with C<sub>22</sub> bonded phases. Four materials were prepared using two different silanes as well as solution and surface polymerization approaches. <sup>29</sup>Si CP/MAS NMR, <sup>13</sup>C CP/MAS NMR, and high-speed <sup>1</sup>H MAS NMR experiments were used to characterize chain conformational structure and dynamic aspects. Steady-state and time-resolved fluorescence anisotropy measurements were employed to investigate the mobility of sorbed probe molecules within the bonded phase, and additional fluorescence spectra and fluorescence lifetime measurements were carried out to determine the fraction of solute partitioning into the alkyl phase. Finally, separations of “shape-selective” probe compounds were performed on corresponding LC columns for correlation of chromatographic retention behavior with the measured physical properties.

### Experimental Section<sup>91</sup>

**Materials Preparation.** The polymeric synthesis procedures of bonded phases have been described elsewhere in detail<sup>2,24</sup> and can be summarized as follows. The term “solution polymerization” describes a procedure in which the di- or trifunctional silane is reacted with a slurry of silica in xylene with the addition of water. When water is added, the silane is hydrolyzed and polymerized in solution. The resulting modified silica surfaces have been characterized as silane clusters or patches.<sup>26</sup> “Surface polymerization” denotes a strategy in which silanes are reacted with humidified silica gel (i.e., silica with a physically adsorbed water monolayer) in an attempt to obtain self-assembled monolayers. In both cases, 3.1 g of YMC silica (YMC Inc., Wilmington, DE, and YMC Europe GmbH, Schermbeck, Germany; pore size 200 Å, particle size 5  $\mu\text{m}$ ) was reacted with 5 mL of the respective dichloromethyl and trichlorodocosyl silane (ABCR GmbH, Karlsruhe, Germany). The reaction conditions and materials properties are summarized in Table 1.

The silane polymers were prepared as follows. Three milliliters of the respective dichloro- or trichlorosilane was dissolved in 30 mL of xylene. Next, 0.5 mL of water was added, and the reaction mixture was refluxed for 2 h. After the mixture was cooled to room temperature, the silane polymer was allowed to dry on a glass plate.

**Solid-State NMR Spectroscopy.** <sup>29</sup>Si CP/MAS NMR measurements were carried out with a Bruker MSL 200 spectrometer (Bruker GmbH, Rheinstetten, Germany). Magic angle spinning was executed at 3500 Hz. <sup>1</sup>H 90° pulses and contact times were 7.7  $\mu\text{s}$  and 5 ms, respectively, with recycle delay times of 1 s.

<sup>13</sup>C CP/MAS and high-speed <sup>1</sup>H MAS NMR experiments were performed by use of a Bruker ASX 300 instrument. For <sup>13</sup>C spectra, sample spinning was executed at 4000 Hz, the proton 90° pulse length was 4.0  $\mu\text{s}$ , and the contact times and delay times were 6 ms and 1 s,

(66) Montgomery, M. E.; Green, M. A.; Wirth, M. J. *Anal. Chem.* **1992**, *64*, 1170–1175.

(67) Pursch, M.; Strohschein, S.; Händel, H.; Albert, K. *Anal. Chem.* **1996**, *68*, 386–393.

(51) Lakowicz, J. R. *Principles of Fluorescence Spectroscopy*; Plenum: New York, 1983.

(52) Lochmüller, C. H.; Colborn, A. S.; Hunnicutt, M. L.; Harris, J. M. *J. Am. Chem. Soc.* **1984**, *106*, 4077–4082.

(53) Lehr, B.; Egelhaaf, H.-J.; Fritz, H.; Rapp, W.; Bayer, E.; Oelkrug, D. *Macromolecules* **1996**, *29*, 7931–7936.

(54) Rutan, S. C.; Harris, J. M. *J. Chromatogr. A* **1993**, *656*, 197–215.

(55) Burns, J. W.; Bialkowski, D. B.; Marshall, D. B. *Anal. Chem.* **1997**, *69*, 3861–3870.

(56) Stahlberg, J.; Algren, M. *Anal. Chem.* **1985**, *57*, 817–821.

(57) Carr, J. W.; Harris, J. M. *Anal. Chem.* **1986**, *58*, 626–631.

(58) Carr, J. W.; Harris, J. M. *Anal. Chem.* **1987**, *59*, 2547–2550.

(59) Lochmüller, C. H.; Marshall, D. B.; Wilder, D. R. *Anal. Chim. Acta* **1981**, *130*, 31–42.

(60) Egelhaaf, H.-J.; Oelkrug, D.; Pursch, M.; Albert, K. *J. Fluoresc.* **1997**, *7*, 311–316.

(61) Hartner, K. C.; Carr, J. W.; Harris, J. M. *Appl. Spectrosc.* **1989**, *43*, 81–87.

(62) Wong, A. L.; Hunnicutt, M. L.; Harris, J. M. *Anal. Chem.* **1991**, *63*, 1076–1081.

(63) Bogar, R. G.; Thomas, J. C.; Callis, J. B. *Anal. Chem.* **1984**, *56*, 1080–1084.

(64) Stahlberg, J.; Algren, M.; Alsins, J. *Anal. Chem.* **1988**, *60*, 2487–2493.

(65) Rangnekar, V. M.; Foley, J. T.; Oldham, P. B. *Appl. Spectrosc.* **1992**, *46*, 827–831.

respectively. High-speed  $^1\text{H}$  MAS NMR measurements were performed with a sample spinning rate of 14 000 Hz, the  $90^\circ$  pulse length was  $4.4 \mu\text{s}$ , and the repetition time was set to 4 s. All chemical shifts were referenced externally to tetramethylsilane (TMS).

2D WISE NMR spectra were recorded under the following conditions. MAS was performed at 4000 Hz. The contact time was set to  $500 \mu\text{s}$  to reduce spin-diffusion, and the pulse repetition time was 1 s. The increment along F1 was set to  $3 \mu\text{s}$ , and typically 80 rows were acquired. Data processing was performed along F2 with exponential multiplication and along F1 with a square cosine function, after zero-filling to 256 data points. The processing of the spectra was performed using Bruker XWINNMR and WIN NMR software.

**Fluorescence Spectroscopy.** All fluorescence measurements were carried out on suspensions which were prepared by adding 4 mg of the RP material to  $10^{-7} \text{ mol}\cdot\text{L}^{-1}$  solutions of DPH in 3.0 mL of acetonitrile (UVASOL, Merck)/water mixtures (2:1, 1:1, and 1:2 v/v). At this silica concentration, no fluorescence depolarization by multiple light scattering was observed. The suspensions were agitated with a magnetic stirrer to prevent sedimentation. Steady-state fluorescence spectra and fluorescence anisotropy spectra were recorded on a SPEX 222 fluorometer equipped with Glan-Thompson polarizers. (Instruments S.A., Longjumeau, France).

Fluorescence decay curves were obtained by applying the single-photon counting technique. A thyatron-controlled nanosecond flashlamp (EI-199F, Edinburgh Instruments, Edinburgh, UK) was used as the light source. Time-resolved anisotropy decay curves were obtained at the Center for Fluorescence Spectroscopy in Baltimore, MD, by single-photon counting. A cavity-dumped, frequency-doubled pyridine 1 laser was used ( $\lambda_{\text{ex}} = 360 \text{ nm}$ ,  $\text{fwhm} = 7 \text{ ps}$ ) as the excitation source. A microchannel plate photomultiplier (R2809, Hamamatsu Photonics, Hamamatsu City, Japan) provided an instrument response of approximately 60 ps.

**Liquid Chromatography (LC).** The separations were performed on a Varian 9012 liquid chromatograph (Varian Inc., Walnut Creek, CA) and a Merck Hitachi L-6200 A instrument (Merck KGaA, Darmstadt, Germany). Standard Reference Material (SRM) 869 (Column Selectivity Test Mixture for Liquid Chromatography) and SRM 1647c (Priority Pollutant Polycyclic Aromatic Hydrocarbons) were obtained from the Standard Reference Materials Program (NIST, Gaithersburg, MD). Other solutes used in the evaluation of shape selectivity were obtained from the following sources: tetraphenylmethane, 1,6-diphenylhexatriene, triphenylene, and triptycene from Aldrich Chemical Co. Inc. (Milwaukee, WI); pyrene and 1,3,5-triphenylbenzene from Fluka Chemical Co. (Ronkonkoma, NY); and *p*-terphenyl from Eastman Organic Chemicals (Rochester, NY).  $\beta$ -Carotene was obtained from Sigma (St. Louis, MO) and BASF AG (Ludwigshafen, Germany) and isomerized using the approach of Zechmeister and Polgar.<sup>68</sup> HPLC grade solvents were used in all chromatographic separations. Absorbance detection was performed at 254 nm for PAH solutes and at 450 nm for  $\beta$ -carotene isomers.

**LC-NMR Experiments.** LC-NMR investigations have been carried out using a Bruker (Rheinstetten, Germany) AMX 600 instrument. The chromatographic equipment and the BPSU (Bruker peak sampling unit) were controlled by Chromstar software (Bruker). An LC inverse probe with a detection volume of  $120 \mu\text{L}$  was chosen for recording of stopped-flow  $^1\text{H}$  NMR spectra. Solvent suppression was done by presaturation of the acetone resonance for 1.2 s prior to acquisition of the free induction decay (FID).

## Results and Discussion

**Materials Characterization. (i) Solid-State NMR Spectroscopy.** Silane functionality and bonding chemistry can easily be determined by  $^{29}\text{Si}$  CP/MAS NMR spectroscopy. NMR spectra of the  $\text{C}_{22}$  phases and the native silica are shown in Figure 1. The signal assignment of silyl fragments can be summarized briefly: a higher degree of cross-linking of silicon species and/or an increase of oxygen neighbors leads to an

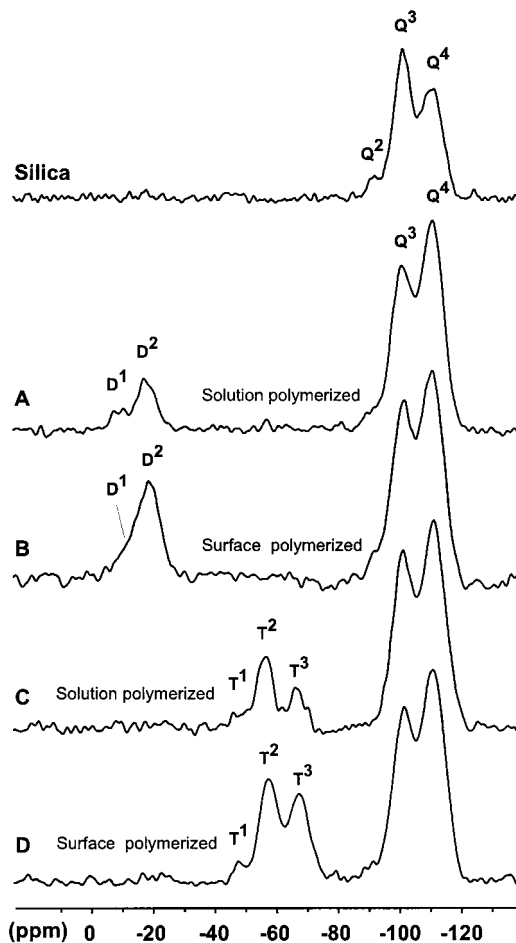
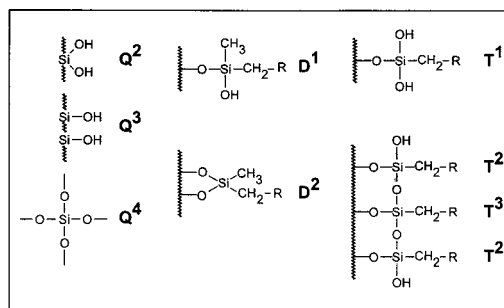


**Figure 1.**  $^{29}\text{Si}$  CP/MAS NMR spectra of  $\text{C}_{22}$  interphases and the native silica gel, including structural assignment.

upfield shift in NMR spectra. Difunctional species ( $\text{D}^n$ ) appear in the region from  $-7$  to  $-20$  ppm, trifunctional species ( $\text{T}^n$ ) from  $-49$  to  $-66$  ppm, and signals from the native silica ( $\text{Q}^n$ ) from  $-91$  to  $-110$  ppm. The ratio of  $\text{Q}^3/\text{Q}^4$  is quite similar for all four interphases, but for surface polymerized materials (**B** and **D**) a higher degree of cross-linking is found (intense  $\text{D}^2$  and  $\text{T}^3$  peaks, respectively). This is probably a consequence of the higher surface coverage. It should be noted that the SAM phase **D** exhibits  $\text{T}^1$  and  $\text{T}^2$  signals, and a fully cross-linked monolayer would be expected to show only  $\text{T}^3$  peaks. This may be due to steric hindrance of the attached long alkyl chains. A  $\text{C}_{18}/\text{C}_1$  horizontally polymerized phase exhibited almost only  $\text{T}^3$  units; however, methyl groups require less space than  $\text{C}_{22}$  chains. As discussed below, studies on silane polymers show that these materials exhibit ordered structures, despite the presence of  $\text{T}^1/\text{T}^2$  signals.<sup>69</sup>

(68) Zechmeister, L.; Polgar, A. *J. Am. Chem. Soc.* **1943**, *65*, 1522–1528.

(69) Shimojima, A.; Sugahara, Y.; Kuroda, K. *Bull. Chem. Soc. Jpn.* **1997**, *70*, 2847–2853.

**Table 2.** Line Widths (Hz)<sup>a</sup> and Coverage (μmol/m<sup>2</sup>) of C<sub>22</sub> Interphases Evaluated from High-Speed <sup>1</sup>H MAS NMR Spectra (14 000-Hz Spinning)

phase	CH <sub>2</sub> (1.2 ppm)	CH <sub>3</sub> (0.8 ppm)	coverage
A	54 (3)	43 (2)	3.61
B	80 (4)	68 (3)	4.65
C	91 (4)	65 (3)	4.89
D	146 (7)	125 (6)	6.97

<sup>a</sup> One standard deviation of the mean is given in parentheses.

Line widths of the CH<sub>2</sub> and CH<sub>3</sub> signals in <sup>1</sup>H MAS NMR spectra (14 000 Hz spinning) of the four different materials are summarized in Table 2. At these spinning speeds, homonuclear dipolar interactions among the immobilized chains are strongly reduced, and two signals are visible. The more intense signal at 1.2 ppm is due to the abundant CH<sub>2</sub> units, and the lower signal at 0.8 ppm characterizes the terminal methyl group. The Si-CH<sub>3</sub> group normally has a resonance close to 0.0 ppm. However, due to the restricted mobility of this fragment close to the silica surface, the peak is strongly broadened (increased dipolar interactions) and is almost undetectable. It is evident that mobility of alkyl chain ligands is reduced with increasing surface coverage.<sup>26</sup> Extremely large line widths under MAS conditions are measured for the high-loaded phase **D** (6.97 μmol/m<sup>2</sup>), and one can conclude that the C<sub>22</sub> ligands possess a very high order. Peak deconvolution showed that the ratio of CH<sub>2</sub>/CH<sub>3</sub> integrals is lower than expected for the high-loaded phases. It seems that some regions of the chains (probably close to the silica surface) possess very short T<sub>2</sub> (transversal relaxation) times; thus, only a fraction of the alkyl chains is detectable.

More detailed information on bonded phase architecture is obtained from <sup>13</sup>C CP/MAS NMR spectra and a few details of alkyl chain order on silica will be discussed briefly. The NMR investigation of C<sub>30</sub> bonded phases exhibits two signals for the main chain methylene carbons.<sup>67,70</sup> One signal at 32.6 ppm is attributed to ordered trans conformations, whereas the other signal at 30.0 ppm is attributed to gauche defects (i.e., an equilibrium of trans and gauche conformations<sup>15</sup>), indicating a partial disorder of the attached ligands. With increasing temperature and with reduced ligand density, the fraction of trans conformations is reduced.<sup>26,67</sup> A clear trend is observed in NMR spectra of bonded phases with extended alkyl chains (C<sub>18</sub> to C<sub>34</sub>): alkyl chain order is found to increase with increasing chain length.<sup>71</sup> It should be noted here that CP/MAS experiments are not quantitative; especially the signal intensity of mobile regions (e.g., trans/gauche conformations) can be distorted by T<sub>1ρH</sub> effects, as well as by the choice of the contact time. Other contributions include relaxation to the lattice of the cross-polarizing signal, the rate of CP (residual C-H couplings), and the radio frequency match. However, contact time variation investigations on long-chain bonded phases (prepared by solution polymerization) showed that CP experiments with contact times of 6 ms and single pulse excitation measurements yield similar trans and trans/gauche signal ratios.

The differences among the four C<sub>22</sub> interphases are clearly evident (Figure 2). For the methylene main chain, two signals are observed, and their ratio is dependent on coverage, bonding chemistry, and temperature. Whereas the C<sub>22</sub> chains of phase **A** (3.61 μmol/m<sup>2</sup>) are predominantly in trans/gauche conformations (signal at 30.0 ppm) at 295 K, the spectra of materials

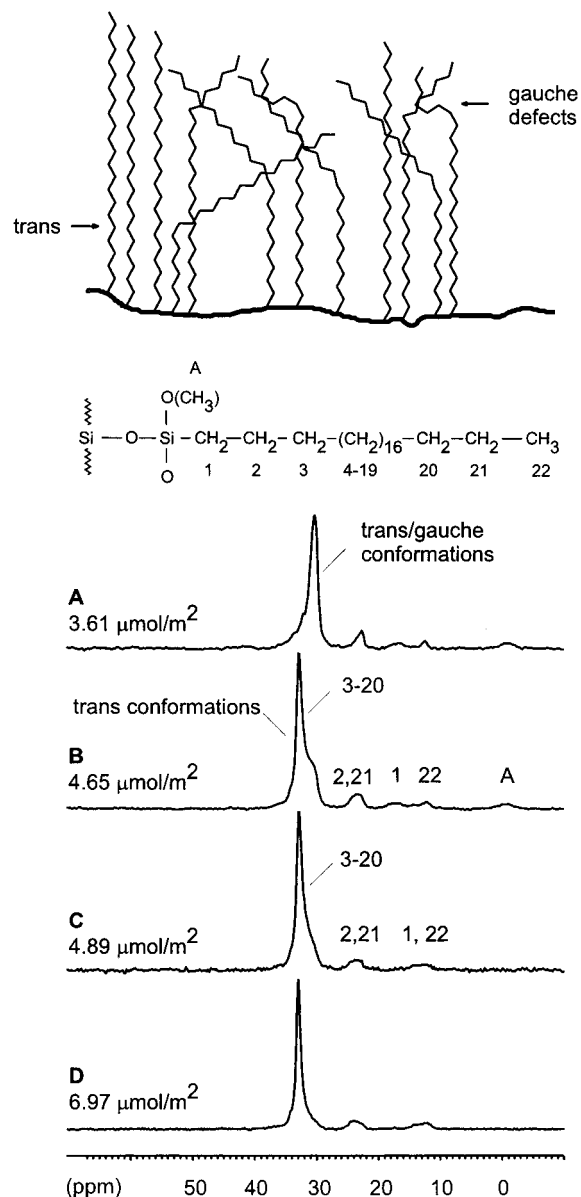


**Figure 2.** <sup>13</sup>C CP/MAS NMR spectra of samples **A–D** obtained at 295 K, including the structure of the C<sub>22</sub> ligand and a schematic illustration of trans and gauche alkyl chain arrangements.

**B–D** are dominated by an intense signal at 32.6 ppm (trans conformations) and a small shoulder at 30.0 ppm. The fraction of gauche defects is reduced with increasing coverage. By comparison, NMR spectra of C<sub>18</sub> phases (on the same type of silica) revealed the presence of a majority of trans conformations (main signal at 32.4 ppm) only for a high-loaded material (coverage greater than 5.5 μmol/m<sup>2</sup>).<sup>26</sup> Although the C<sub>22</sub> chain is only 22% longer than a C<sub>18</sub> ligand, this extension has dramatic effects on alkyl chain order. This has also been noticed by Morel and Serpinet while studying monomeric C<sub>22</sub> phases in gas chromatography (GC)<sup>72</sup> and LC.<sup>73</sup> It is interesting to note that the self-assembled monolayer phase **D** (6.97 μmol/m<sup>2</sup>) shows a very sharp resonance at 32.6 ppm, and no trans/gauche conformations are found. This characteristic is very similar to that of self-assembled monolayers of C<sub>18</sub> ligands on gold or silicon substrates. Solid-state NMR investigations on these materials also exhibited a main low-field signal (32.5–33.0

(70) Albert, K.; Händel, H.; Pursch, M.; Strohschein, S. In *Chemically Modified Surfaces*; Pesek, J. J., Matyska, M. T., Abuelafiya, R. R., Eds.; The Royal Society of Chemistry: Cambridge, UK, 1996; pp 30

(71) Pursch, M.; Brindle, R.; Ellwanger, A.; Sander, L. C.; Bell, C. M.; Haendel, H.; Albert, K. *J. Solid State NMR Spectrosc.* **1997**, *9*, 191–201.

(72) Morel, D.; Serpinet, J. *J. Chromatogr.* **1981**, *214*, 202–208.

(73) Morel, D.; Serpinet, J. *J. Chromatogr.* **1982**, *248*, 231–240.

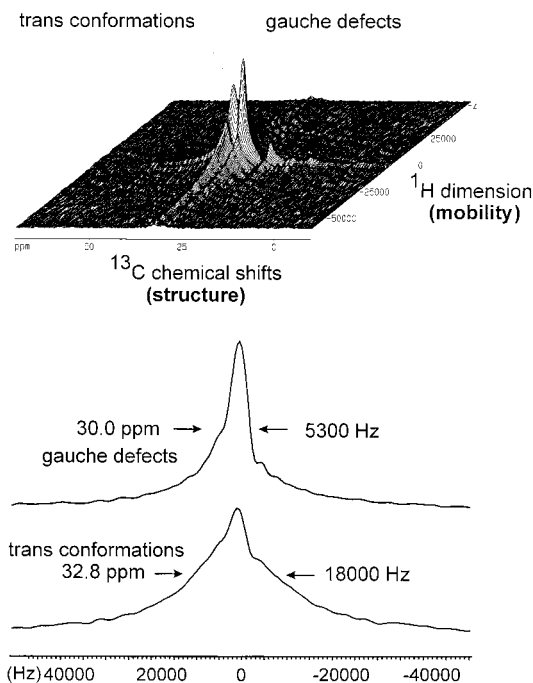


**Figure 3.** 2D WISE NMR spectrum of phase **B** ( $4.65 \mu\text{mol}/\text{m}^2$ ) measured at 315 K. The lower spectra were obtained by extracting a slice at 32.8 ( $^1\text{H}$  dimension) and 30.0 ppm ( $^{13}\text{C}$  dimension), respectively.

ppm) for the methylene chains, which is indicative of an ordered surface.<sup>12,15,16</sup>

A 2D WISE experiment was utilized to characterize the dynamic behavior of trans and gauche conformations of interphase **B** (Figure 3). In this sequence, a  $90^\circ$  proton excitation pulse is followed by an incremented delay, in which magnetization of the different chain fragments is subject to transverse relaxation ( $T_2$ ) in the  $x,y$ -plane. The residual  $^1\text{H}$  magnetization is then transferred via cross polarization to carbon nuclei, and the resulting FID is acquired. High rigidity or strong dipolar couplings lead to very short  $T_2$  times and thus to broad line widths in the  $^1\text{H}$  dimension. This experiment combines the high signal resolution of  $^{13}\text{C}$  nuclei (increased chemical shift range of carbon fragments) with the individual mobility of its associated protons, thus providing a measure of local mobility. The fact that a  $500\text{-}\mu\text{s}$  CP time was used allows for some mixing (via spin diffusion) between mobile and rigid regions, provided that these mobility differences exist over distances of 0.6–0.7 nm, the distance that spin-diffusion would cover for a rigid alkane.

From the 2D NMR spectrum displayed in Figure 3, differences in the dynamic conformational behavior of the alkyl chains are quite obvious. The trans conformations ( $^1\text{H}$  line width 18 000 Hz) are more rigid than the gauche defects ( $^1\text{H}$  line width 5300 Hz). The WISE NMR experiment confirms the results of the one-dimensional NMR spectra and provides information on the mobility of the respective conformations. Dramatic differences in conformational mobility are clearly apparent in the WISE NMR spectra of phases **A** and **D** (Supporting Information). Whereas phase **A** exhibits a fairly narrow signal in the proton dimension (9000 Hz) corresponding to disordered alkyl chains, the SAM phase **D** (proton line width 34 000 Hz) has very rigid and ordered  $\text{C}_{22}$  ligands. These data show that silane functionality and synthesis method have a strong influence on the structure and dynamic behavior of immobilized alkyl chains.

It was also worthwhile to study the NMR properties of difunctional and trifunctional  $\text{C}_{22}$  silane polymers (Figure 4).

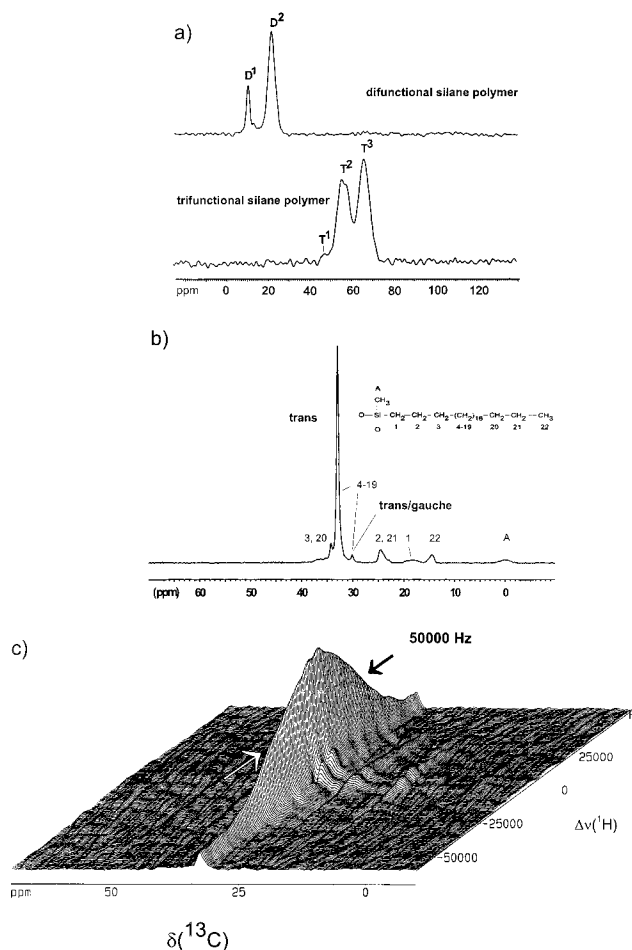


**Figure 4.** Solid-state NMR characterization of  $\text{C}_{22}$  silane polymers. (a)  $^{29}\text{Si}$  CP/MAS NMR, (b)  $^{13}\text{C}$  CP/MAS NMR, and (c) 2D WISE NMR. The sample in spectra b and c is a difunctional silane polymer.

From the silicon NMR spectra, the presence of D and T silanols shows that complete cross-linking did not occur, probably due to steric effects. Because the  $^{13}\text{C}$  NMR spectra of these two compounds are similar, only the results for the difunctional silane polymer are shown. As is expected, these materials exhibit a high degree of chain order, comparable to that of silanized silica with very high bonding density (e.g., self-assembled monolayer phase **D**). The main  $^{13}\text{C}$  CP/MAS NMR signal appears at 33.0 ppm, corresponding to trans conformations. Although the peak width of this signal is quite narrow, the large proton line width in the 2D WISE spectrum (50 000 Hz) confirms the high rigidity and structural order of the hydrocarbon chains. Similar findings were reported by Parikh et al.<sup>74</sup> Their X-ray diffraction and IR studies of layered crystals formed by hydrolysis of octadecyltrichlorosilane showed that the alkyl chain arrangement is highly organized, similar to that of self-assembled monolayers on hydrophilic substrates.

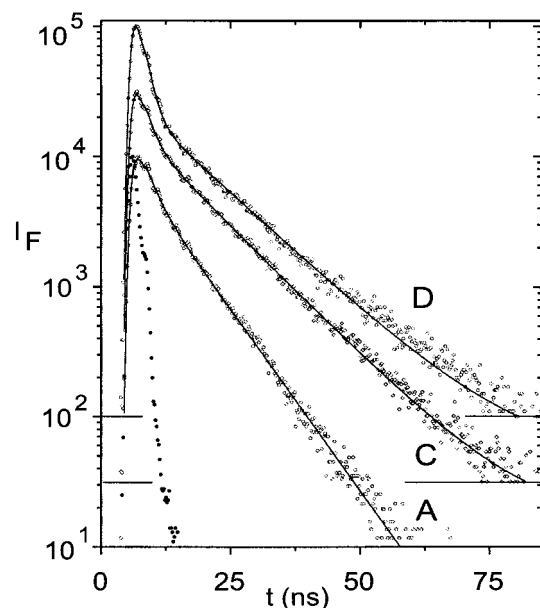
**(ii) Fluorescence Spectroscopy. (a) Fluorescence Probes.** Solid-state NMR measurements provide information on the structure and mobility of the grafted chains. Fluorescence spectroscopy provides a sensitive approach to assess the effect of the bonded phase structure on partitioning and mobility of the solute molecules. The fluorescent probe used in the present studies is DPH. Fluorescence lifetimes were obtained from a

(74) Parikh, A. N.; Schivley, M. A.; Koo, E.; Seshadra, K.; Aurentz, D.; Mueller, K.; Allara, D. L. *J. Am. Chem. Soc.* **1997**, *119*, 3135–3143.

(75) Bondarev, S. L.; Bachilo, S. M. *J. Photochem. Photobiol.* **1991**, *59*, 273–278.

**Table 3.** Fluorescence Lifetimes,  $\tau_F$ , and Quantum Yields,  $\phi_F$ , of DPH in Different Degassed Solvents<sup>a</sup>

solvent	$\tau_F$ (ns)	$\phi_F$
<i>n</i> -decane	14.0	0.68
<i>n</i> -butanol	8.1	0.35
ethanol	5.6	0.26
acetonitrile	4.1	0.17
acetonitrile/water (1:2)	1.2	0.04

<sup>a</sup>Data for pure solvents are taken from ref 75.**Figure 5.** Fluorescence decay curves of DPH in suspensions of three different C<sub>22</sub> phases (A, C, and D) in acetonitrile/water mixtures (1:1 v/v). The decay curves have been offset vertically for the sake of clarity. The fluorescence decay curve of phase B is very similar to that of phase D and has, therefore, been omitted. Filled dots represent the profile of the exciting flashlamp.

double-exponential analysis of the fluorescence decay curves,  $I_F(t)$ ,

$$I_F(t) = \sum_i A_i \exp(-t/\tau_{F,i}) \quad (1)$$

where  $\tau_{F,i}$  represents the decay time of the *i*th component and  $A_i$  is the amplitude of the components decay curve, i.e., its intensity at  $t = 0$ . The fluorescence lifetime and quantum yield for this probe have been shown to be a sensitive function of the microenvironment, as indicated in Table 3. For example, the fluorescence lifetime of DPH in water/acetonitrile mixtures is  $\tau_F \approx 1.2$  ns, whereas it is considerably longer in hydrocarbon environments. This sensitivity results from the enhancement of radiative rates with increasing polarizability of the medium and the enhancement of nonradiative rates with increasing polarity of the medium.<sup>75</sup> In addition, increased polarizability of the environment causes a red shift of the fluorescence excitation maxima.

**(b) Effect of Ligand Density.** The fluorescence decay curves of DPH in each of the C<sub>22</sub> phases (Figure 5) are well approximated by biexponential fits, with  $\tau_F \approx 1.3$  ns and  $\tau_F \approx 5-8$  ns. The short-decay component is similar to that observed with acetonitrile/water mixtures and is attributed to DPH in the mobile phase, whereas the long-decay component is assigned to DPH in the alkyl phase. Although the short-decay component is practically independent of the stationary phase properties, the fluorescence lifetime of sorbed DPH increases with increasing

ligand density up to a surface coverage of 4.9  $\mu\text{mol}/\text{m}^2$  and decreases again for the highest surface coverage. The enhancement of the fluorescence decay time of DPH upon sorption into the alkyl phase indicates a lower polarity of the interphase compared to that of the mobile phase. This nonpolar environment results from the nonpolar alkyl ligands and from preferential sorption of acetonitrile into the alkyl layer (from the acetonitrile/water mobile phase).<sup>56-58</sup> The interphase polarity decreases further with increasing ligand density. A comparison of the fluorescence lifetimes in Tables 3 and 4 reveals that bonded phase polarity decreases from a value similar to that for acetonitrile for phase A, to a value comparable to that for *n*-butanol for phase C. The deviation of sample phase D is due to the fact that DPH is not capable of penetrating between the densely packed alkyl chains, as will be discussed below. The decrease in polarity of the interphase with increasing surface coverage is accompanied by an increase of the polarizability, as can be deduced from the red shift of the maxima of the fluorescence excitation spectra of DPH. Again, phase D does not follow this trend. Its red shift is considerably smaller than that of phase C, indicating that the fraction of DPH molecules shielded from the bulk mobile phase is much lower in phase D than it is in phase C.

The mole fractions of DPH sorbed in the interphase,  $x_s$ , can be calculated by employing eq 2.  $x_j$  of the species associated with the decay component *j* is given by

$$x_j = \frac{A_j \tau_{F,j} \phi_{F,j}^{-1}}{\sum_i A_i \tau_{F,i} \phi_{F,i}^{-1}} \quad (2)$$

where  $\phi_{F,i}$  is the fluorescence quantum yield of the *i*th fluorescing species, and the extinction coefficients,  $\epsilon_i$ , of all species are equal.

Because the exact value of the fluorescence quantum yield of DPH in the alkyl phase is not known, we have estimated  $\phi_F = 0.26$ , which is the value for DPH in ethanol. The polarity and polarizability of alkyl interphases are thought to be similar to those of ethanol. The resulting calculated mole fractions of DPH for the four C<sub>22</sub> phases are listed in Table 4. It is clear that the partitioning behavior of DPH is not a simple function of the ligand density. The partition coefficient increases with increasing ligand density until a maximum is reached (phase C). The partition coefficient decreases for the highest loaded phase (phase D). A similar trend has also been observed by Sentell and Dorsey.<sup>76</sup> They have studied retention behavior of naphthalene on monomeric C<sub>18</sub> phases and found a maximum in partition coefficient at a bonding density of 3.1  $\mu\text{mol}/\text{m}^2$ .

Fluorescence anisotropy measurements provide insight into the mobility of DPH in the interphase. Anisotropy decay curves  $r(t)$  were obtained from

$$r(t) = D(t)/S(t) \quad (3)$$

where  $D(t) = I_{vv}(t) - gI_{vh}(t)$  and  $S(t) = I_{vv}(t) + 2gI_{vh}(t)$ . The scaling factor  $g = I_{hv}/I_{hh}$  was determined for each experiment.  $I_{vv}$ ,  $I_{vh}$ ,  $I_{hv}$ , and  $I_{hh}$  stand for the observed fluorescence intensities, where first and second indices indicate the positions (*v* = vertical, *h* = horizontal) of polarizer and analyzer, respectively. In the case of a single fluorescing species, the decay of the fluorescence anisotropy,  $r(t)$ , after a short laser pulse is exponential:

(76) Sentell, K. B.; Dorsey, J. G. *Anal. Chem.* **1989**, *61*, 930-934.

**Table 4.** Photophysical Data of DPH in Suspensions of Four Different C<sub>22</sub> Phases<sup>a</sup>

phase	$\tau_{F,m}$ (ns)	$A_m$	$\tau_{R,m}$ (ns)	$\tau_{F,s}$ (ns)	$A_s$	$\tau_{R,s}$ (ns)	$\theta$ (deg)	$x_s$	$\nu_{max}$ (cm <sup>-1</sup> )
<b>A</b>	1.24 (0.02)	0.85 (0.02)	0.18 (0.01)	4.66 (0.06)	0.15 (0.01)	1.0 (0.02)	59	0.10	28 230 (20)
<b>B</b>	1.30 (0.03)	0.92 (0.02)	0.18 (0.01)	6.42 (0.06)	0.08 (0.01)	1.0 (0.02)	43	0.06	
<b>C</b>	1.39 (0.03)	0.82 (0.02)	0.18 (0.01)	8.05 (0.08)	0.18 (0.01)	1.2 (0.02)	36	0.17	28 160 (20)
<b>D</b>	1.31 (0.03)	0.92 (0.02)	0.18 (0.01)	6.22 (0.06)	0.08 (0.01)	1.0 (0.02)	43	0.06	28 360 (20)

<sup>a</sup> One standard deviation of the mean is given in parentheses. The indices “m” and “s” designate DPH in the mobile and stationary phases, respectively. Fluorescence lifetimes,  $\tau_F$ , and amplitudes,  $A$ , were obtained from the biexponential analysis of the fluorescence decay curves. Rotational correlation times,  $\tau_R$ , and half-cone angles,  $\theta$ , were obtained from the analysis of the fluorescence anisotropy decay curves.  $x_s$  is the mole fraction of DPH sorbed in the interphase, calculated according to eq 2. The maxima of the fluorescence excitation spectra,  $\nu_{max}$ , are listed in the last column.

$$r(t) = (r_0 - r_\infty) e^{-t/\tau_R} + r_\infty \quad (4)$$

where  $r_0$  is the anisotropy at  $t = 0$ ,  $\tau_R$  is the rotation correlation time, and  $r_\infty$  is the residual anisotropy for  $t \rightarrow \infty$ . For unrestricted motion,  $r_\infty = 0$ . If the diffusional motion of the fluorophore is restricted to a solid cone (“wobble-in-cone”; see the inset in Figure 6),

$$\frac{r_\infty}{r_0} = [0.5 \cos \theta (\cos \theta + 1)]^2 \quad (5)$$

where  $\theta$  is the half-cone angle, as defined in Figure 6.

If several fluorescing species,  $i$ , are present, with different rotation correlation times,  $\tau_{R,i}$ , and different fluorescence lifetimes,  $\tau_{F,i}$ , then the decay is described by

$$r(t) = \frac{\sum_i I_{F,i}(t) r_i(t)}{\sum_i I_{F,i}(t)} = \frac{\sum_i A_i e^{-t/\tau_{F,i}} [(r_{0,i} - r_{\infty,i}) e^{-t/\tau_{R,i}} + r_{\infty,i}]}{\sum_i A_i e^{-t/\tau_{F,i}}} \quad (6)$$

Figure 6 shows the fluorescence anisotropy decay curves of DPH in three different phases. The presence of minima in the curves indicates associated decays of two species. The species with the longer fluorescence decay time,  $\tau_F$ , also possesses the longer rotational correlation time,  $\tau_R$ . Fitting of the curves to eq 6 yields the data listed in Table 4. To reduce the number of adjustable parameters in the fitting procedure, fluorescence decay times and the corresponding amplitudes are taken from the fits of the fluorescence decay curves. Only in the case of phase A, a slight variation of these parameters is necessary to obtain the good agreement between experimental and fitted anisotropy decay curves shown in Figure 6 (the exact values of fluorescence decay times and the respective amplitudes used in the fitting of fluorescence anisotropy traces are available in the Supporting Information). The rotational correlation time for DPH in the mobile phase is assumed to be equal to that in a solution of the same solvent composition. This leaves two parameters to be determined, i.e., the rotational correlation time and the residual anisotropy for DPH in the interphase.

As can be seen from the data in Table 4, the rotational correlation times in all four phases are very similar, but the residual anisotropies differ appreciably. The half-cone angle determined from the residual anisotropies with eq 5 increases with decreasing ligand density, thus indicating that the space available for the wobbling motion of DPH increases.

**(c) Effect of Liquid Phase Composition.** To elucidate the effect of the composition of the mobile phase on the structure and dynamics of the interphase, fluorescence lifetimes and

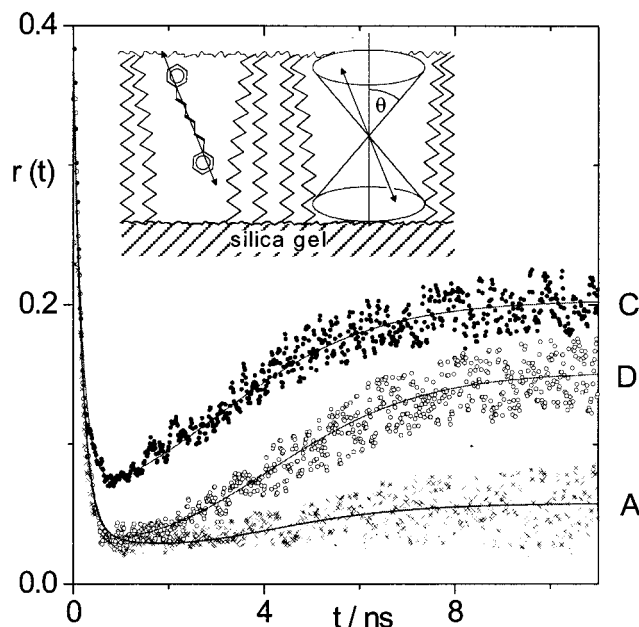


**Figure 6.** Fluorescence anisotropy decay curves of DPH in suspensions of three different C<sub>22</sub> phases (A, C, and D) in acetonitrile/water mixtures (1:1 v/v). The fluorescence anisotropy decay curve of phase B is very similar to that of phase D and has, therefore, been omitted. The inset shows a schematic representation of the studied systems. Silica bonded C<sub>22</sub> chains form the stationary phase. The mobile phase is an acetonitrile/water mixture. The probe molecule, 1,6-diphenylhexatriene (DPH), performs a wobble-like motion in a cone defined by the half-cone angle  $\theta$ , which is determined by the size of the interstices between the alkyl chains.

fluorescence anisotropies of DPH in suspensions of phase C in acetonitrile/water mixtures of different water content are measured. The results of fluorescence lifetime measurements of DPH are summarized in Table 5 (the respective fluorescence anisotropy spectra are included in the Supporting Information). While the fluorescence lifetime of DPH in the mobile phase decreases with increasing water content, the opposite trend is observed for DPH in the stationary phase, indicating that the increased water content in the mobile phase leads to decreased polarity experienced by the DPH molecules sorbed in the interphase. The mobility of DPH sorbed in the interphase is significantly reduced, indicated by the increase of the rotational correlation time,  $\tau_R$ , and the decrease of the half-cone angle,  $\theta$  (Table 5). These results are in accordance with NMR,<sup>77</sup> fluorescence, and LC investigations,<sup>78</sup> which have revealed that the alkyl chains of reversed phases aggregate and may even

(77) Marshall, D. B.; McKenna, W. P. *Anal. Chem.* **1984**, *56*, 2090–2093.

(78) Gilpin, R. K.; Squires, J. A. *J. Chromatogr. Sci.* **1981**, *19*, 195–199.

**Table 5.** Photophysical Data of DPH in Suspensions of Phase C in Solvent Mixtures of Different Water Content (v/v)<sup>a</sup>

H <sub>2</sub> O/ MeCN	$\tau_{F,m}$ (ns)	$A_m$	$\tau_{R,m}$ (ns)	$\tau_{F,s}$ (ns)	$A_s$	$\tau_{R,s}$ (ns)	$\theta$ (deg)	$x_s$
2:1	0.94 (0.02)	0.81 (0.02)	0.23 (0.01)	9.50 (0.08)	0.19 (0.01)	1.6 (0.03)	29	0.27
1:1	1.39 (0.02)	0.82 (0.02)	0.18 (0.01)	8.05 (0.08)	0.18 (0.01)	1.2 (0.02)	36	0.17
1:2	1.52 (0.02)	0.90 (0.02)	0.20 (0.01)	6.47 (0.06)	0.10 (0.01)	0.8 (0.02)	38	0.07

<sup>a</sup>One standard deviation of the mean is given in parentheses. The indices "m" and "s" designate DPH in the mobile and stationary phases, respectively. Fluorescence lifetimes,  $\tau_F$ , and amplitudes,  $A$ , obtained from the biexponential analyses of the fluorescence decay curves. Rotational correlation times,  $\tau_R$ , and half-cone angles,  $\theta$ , were obtained from the analysis of fluorescence anisotropy decay curves.  $x_s$  is the mole fraction of DPH sorbed in the interphase, calculated according to eq 2.

collapse onto the silica surface at high water content of the mobile phase. The fraction of DPH in the interphase increases with increasing water content, as calculated from the areas under the fluorescence decay curves and the fluorescence quantum yields according to eq 2. As in the previous section,  $\phi_F = 0.04$  and 0.26 are inserted for the fluorescence quantum yields of DPH in the mobile and stationary phases, respectively.

**(iii) Liquid Chromatography (LC).** Each of the C<sub>22</sub> stationary phases was characterized with SRM 869,<sup>79</sup> a shape selectivity test mixture consisting of 1,2-3,4-5,6-7,8-tetrabenzonaphthalene (TBN), phenanthro[3,4-*c*]phenanthrene (PhPh), and benzo[*a*]pyrene (BaP). This empirical test was developed after evaluation of over 100 PAH solutes; the three solutes selected provided the most sensitive indication of changes in selectivity due to solute shape. In previous work on C<sub>18</sub> phases, Sander and Wise<sup>24,80</sup> demonstrated that the elution order of these solutes is correlated with the type of surface modification chemistry used to prepare the stationary phases and the overall shape recognition ability. The ratio ( $\alpha$ ) of capacity factors ( $k'$ ) for TBN and BaP (i.e.,  $\alpha_{TBN/BaP} = k'_{TBN}/k'_{BaP}$ ) provides a measure of shape selectivity that is useful for column intercomparisons. Polymeric C<sub>18</sub> columns exhibit a high degree of shape selectivity, and  $\alpha_{TBN/BaP}$  values typically fall within the range of 0.3–1.0. Monomeric columns exhibit lower shape recognition capabilities, and  $\alpha_{TBN/BaP}$  values are usually greater than 1.7. In general, better separations of complex isomer mixtures are possible with polymeric columns compared with those with monomeric columns. We have observed selectivity coefficients with the four C<sub>22</sub> phases ranging from 0.12 (D) to 1.25 (A) (Table 1). Column A exhibits the least shape recognition for PAHs, which is consistent with the shape selectivity test ( $\alpha_{TBN/BaP} = 1.25$ ; TBN elutes after BaP). BaP elutes last with columns B, C, and D, indicating increased shape recognition. The highest degree of shape recognition was observed for the SAM phase D ( $\alpha_{TBN/BaP} = 0.12$ ). As shown by the <sup>13</sup>C CP/MAS NMR studies, this material exhibits a high degree of alkyl chain organization. To better assess selectivity differences of the four columns, an additional extended PAH mixture was composed. Five aromatic solutes were selected on the basis of different molecular shapes: tetraphenylmethane (TPM, spherical), pyrene (planar), 1,3,5-triphenylbenzene (slightly nonplanar), *p*-terphenyl (extended nonplanar), and 1,6-diphenylhexatriene (DPH, extended planar) (Figure 7). Dramatic differences in

(79) Sander, L. C.; Wise, S. A. *Certificate of Analysis, Standard Reference Material 869, Column Selectivity Test Mixture*; NIST: Gaithersburg, MD, 1990.

(80) Sander, L. C.; Wise, S. A. *J. High Resolut. Chromatogr. Chromatogr. Commun.* **1988**, *11*, 383–387.

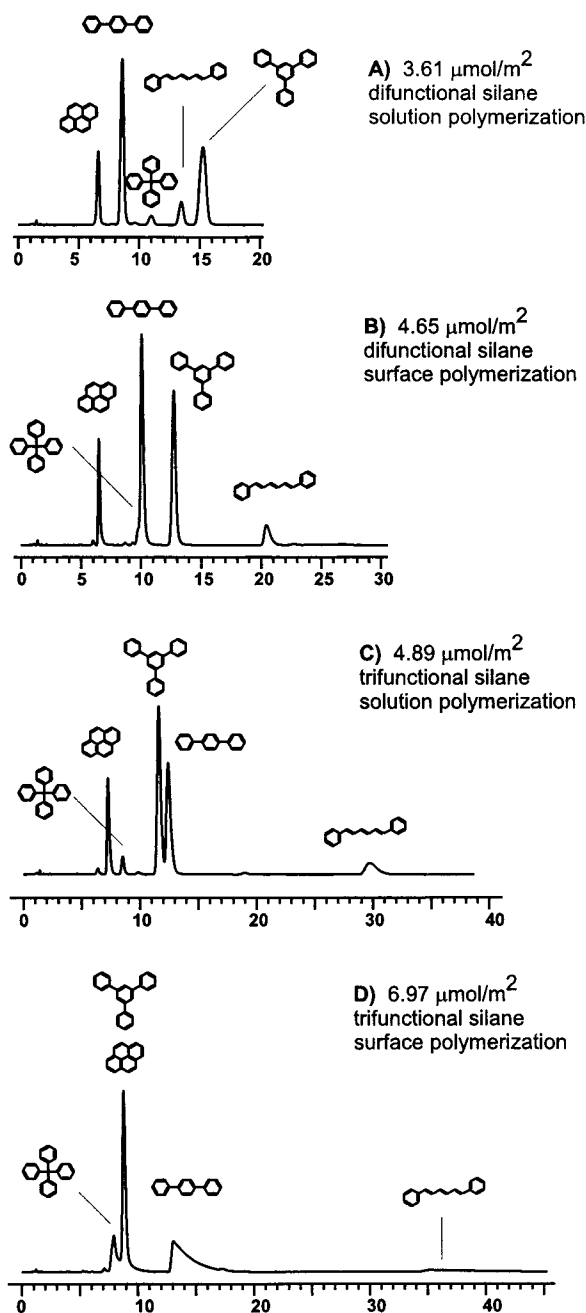


**Figure 7.** Separation of an extended shape selectivity mixture on C<sub>22</sub> interphases. Mobile phase composition, acetonitrile/water 65/35.

selectivity were observed for columns A–D. It is instructive to examine the relative and absolute changes in retention for TPM and DPH among the four columns. The retention of DPH increases with increasing surface coverage and elutes last, except with column A. In contrast, the retention of TPM decreases with increasing surface coverage, and the elution order changes from third (with column A) to first (with column D). The retention of pyrene is nearly unaffected by the changes in bonding density. A correlation of solute shape with the changes in retention that occur for the different columns enables the following observation: the retention of extended solutes increases with increasing bonding density of the stationary phase, relative to more compactly shaped solutes. In contrast, the retention of globular-shaped solutes decreases with increasing bonding density. Peak shape is noticeably degraded for highly retained solutes with densely bonded stationary phases. This behavior may be the

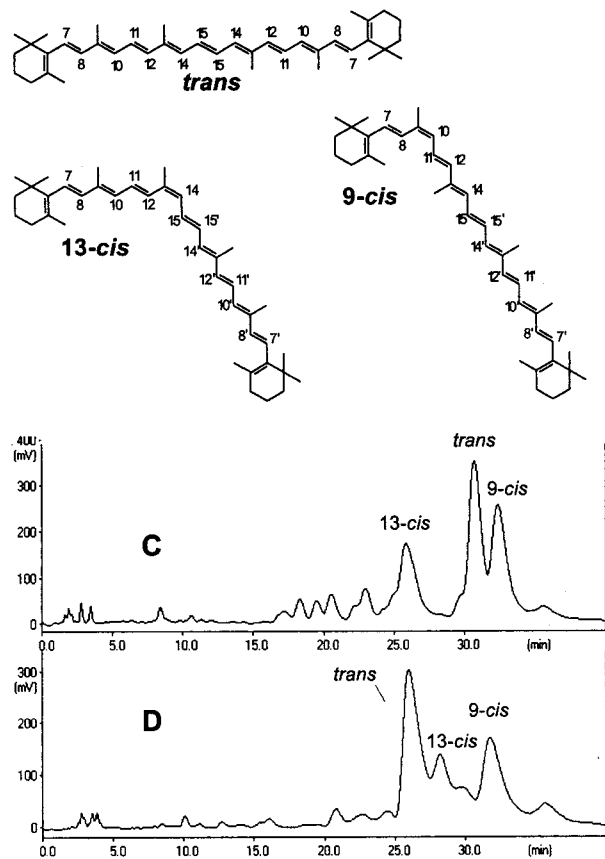


**Figure 8.** Separation of  $\beta$ -carotene isomers on phases **C** and **D**. Mobile phase composition, acetone/water 85/15. Structural assignment was performed by LC-NMR.

result of restricted solute mobility within high-density stationary phases; this was also concluded from fluorescence measurements.

Although it was recently demonstrated that the longer chain  $C_{30}$  bonded phases permit excellent separations of carotenoids and tocopherols compared to  $C_{18}$  sorbents,<sup>8</sup> we have utilized  $\beta$ -carotene isomers as another class of rigid, extended solutes to evaluate selectivity differences among the  $C_{22}$  interphases. As expected, separations of  $\beta$ -carotene isomers on columns **A** and **B** (not shown) were rather poor. Separations of  $\beta$ -carotene on phases **C** and **D** are improved and reveal clear differences in selectivity (Figure 8). Peak assignments were performed by using LC-NMR. For peak identification of structural isomers, LC-NMR<sup>67,81,82</sup> with  $^1\text{H}$  NMR detection is the method of choice, as it offers a very powerful tool for structure elucidation in a closed system that prevents degradation and further isomerization of sensitive compounds (e.g., carotenoids) by oxidation or photolysis. The elution order of the major isomers (13-cis, trans, 9-cis) on interphase **C** is very similar to that of solution-polymerized  $C_{30}$  phases; however, the overall selectivity is reduced due to the shorter  $C_{22}$  chains. Interestingly, the elution order of 13-cis- and trans- $\beta$ -carotene is reversed with column **D**, apparently due to different alkyl chain organization with this column. It should also be noted that the absolute retention times for these isomers are quite similar, despite the differences in surface coverages. This also points to restricted insertion of carotenoid solutes into a very dense and highly organized matrix, as is the case with column **D**.

**Temperature Dependence Studies.** The influence of temperature on conformational changes of immobilized alkyl chains is easily monitored by  $^{13}\text{C}$  solid-state NMR spectroscopy. A comparison of  $^{13}\text{C}$  CP/MAS NMR spectra of phases **B–D** with increasing temperature is provided in Figure 9. Dramatic changes in trans/gauche populations are observed for the different phases. It has been shown for  $C_{30}$  phases that the trans signal at 32.6 ppm is reduced at increased temperature, whereas the signal for trans/gauche conformations (30.0 ppm) is increased.<sup>67,83</sup> However, there is no further upfield shift from the 30.0 ppm signal, which is also the case for melted silane polymers or silanes in solution. The same conformational changes are also observed for phases **B** and **C**; however, these changes occur over a different temperature interval. At room temperature, the alkyl chains of interphase **B** possess more gauche defects than phase **C**. At higher temperatures, the interconversion from trans to gauche occurs sooner for **C** than for **B**, despite the slightly lower surface coverage of the latter. Jinno et al. showed for a polymeric  $C_{18}$  phase a similar temperature-dependent behavior; however, the resolution between trans and gauche signals was lower.<sup>84</sup> The SAM material **D** is also noteworthy with respect to temperature changes. Only a tiny fraction of gauche defects is detected, even at elevated temperatures (up to 355 K). This is further evidence of the very homogeneous, rigid alkyl chain arrangement on the silica surface.

The effect of temperature on the fluorescence decay times of DPH in suspensions of phase **C** in acetonitrile/water mixtures is presented in Figure 10 and Table 6. The most striking effect is the decrease of the mole fraction of DPH sorbed in the interphase with increasing temperature. The values given for the mole fractions are only approximate, because the temperature dependence of the fluorescence quantum yield is estimated. However, as the ratio of the fluorescence quantum yields of the species in mobile and stationary phase varies only little with temperature, the deviation from the exact values is still acceptable. The driving force of the redistribution of DPH with varying temperature between liquid and bonded alkyl phase is the increase in entropy upon ejection of a DPH molecule from the alkyl layer. It is this redistribution which in LC leads to decreasing retention times and loss of selectivity.

Time-resolved fluorescence anisotropy measurements reveal that the half-cone angle  $\theta$  increases with increasing temperature, which indicates that the free volume available for the diffusional motion of DPH increases with increasing temperature. This can easily be understood as a consequence of the disordering of the alkyl chains at higher temperatures.<sup>85</sup> As demonstrated in Table 6, this is not a phase transition in the sense of a sudden two-dimensional melting process of the alkyl layer, but rather is a gradual process extending over a considerable temperature range that results from changes in gauche/trans conformational order. Solid-state NMR investigations support these conclusions as well.

Changes in chromatographic selectivity are clearly evident with changes in temperature. This phenomenon was first reported by Sander and Wise for the separation of polycyclic aromatic hydrocarbons on monomeric and polymeric  $C_{18}$  columns.<sup>85</sup> A general trend was observed for both column types: shape recognition was found to increase with decreasing temperature. Separations of a similar test mixture as described

(83) Albert, K.; Lacker, T.; Raitza, M.; Pursch, M.; Egelhaaf, H.-J.; Oelkrug, D. *Angew. Chem., Int. Ed.* **1998**, *37*, 777–780.

(84) Jinno, K.; Ibuki, T.; Tanaka, N.; Okamoto, M.; Fetzer, J. C.; Biggs, W. R.; Griffiths, P. R.; Olinger, J. M. *J. Chromatogr.* **1989**, *461*, 209–227.

(85) Sander, L. C.; Wise, S. A. *Anal. Chem.* **1989**, *61*, 1749–1754.

(81) Albert, K. *J. Chromatogr. A* **1995**, *703*, 123–147.

(82) Lindon, J. C.; Nicholson, J. K.; Wilson, I. D. *Prog. NMR Spectrosc.* **1996**, *29*, 1–49.

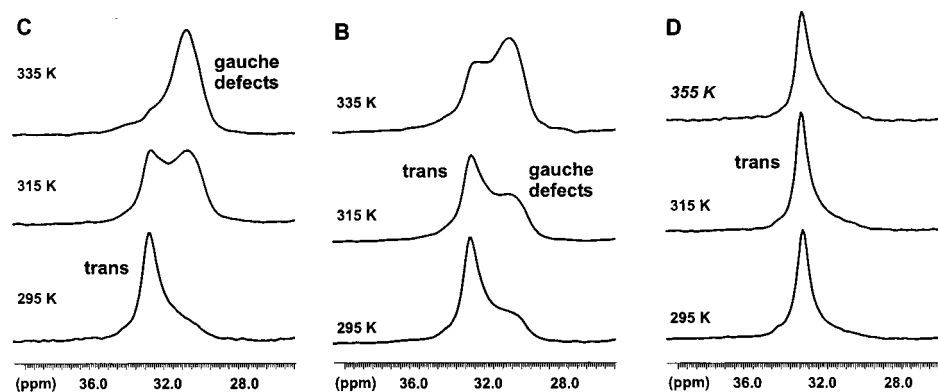


Figure 9. Temperature-dependent <sup>13</sup>C CP/MAS NMR spectra of interphases **B**, **C**, and **D**.

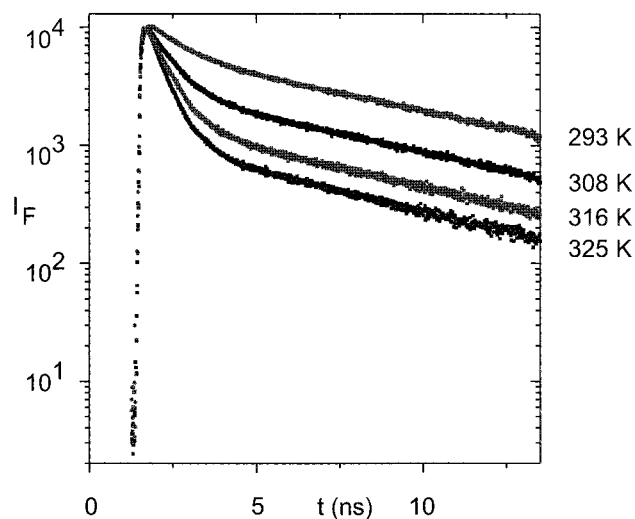


Figure 10. Fluorescence decay curves of DPH in a suspension of phase **C** in acetonitrile/water (1:2 v/v) at different temperatures.

Table 6. Photophysical Data of DPH in Suspensions of Phase **C** in Acetonitrile/ Water Mixtures (1:2 v/v) at Different Temperatures<sup>a</sup>

T (K)	$\tau_{F,m}$ (ns)	$A_m$	$\tau_{F,s}$ (ns)	$A_s$	$x_s$	$\theta$ (deg)
288	1.15 (0.02)	0.42 (0.02)	7.54 (0.07)	0.58 (0.02)	0.58	36
293	1.05 (0.02)	0.52 (0.02)	7.62 (0.07)	0.48 (0.02)	0.51	37
308	0.75 (0.02)	0.78 (0.02)	7.33 (0.07)	0.22 (0.02)	0.30	45
316	0.62 (0.02)	0.89 (0.02)	6.98 (0.07)	0.11 (0.02)	0.18	53
325	0.53 (0.02)	0.96 (0.02)	6.50 (0.07)	0.04 (0.02)	0.07	63

<sup>a</sup>One standard deviation of the mean is given in parentheses. The indices "m" and "s" designate DPH in the mobile and stationary phases, respectively. Fluorescence lifetimes,  $\tau_F$ , amplitudes,  $A$ , and mole fractions of DPH sorbed in the interphase,  $x_s$ , are obtained from the biexponential analyses of the fluorescence decay curves. The half-cone angles,  $\theta$ , are obtained from the analyses of the fluorescence anisotropy decay curves.

in the Liquid Chromatography (LC) section are illustrated in Figure 11 for the four columns, at temperatures ranging from 10 to 50 °C. Selectivity extremes are represented by column **A**, operated at 50 °C (lowest shape recognition), and column **D**, operated at 10 °C (highest shape recognition). The relative retention of triphenylene and 1,6-diphenylhexatriene can be seen to increase relative to those of triptycene and TPM with decreasing temperature. This trend is similar to that described in the LC section and Figure 7 for increases in bonding density. Because alkyl chain conformation changes with temperature, solute interaction with the stationary phase can also be expected to change as bonded phase morphology varies. Such selectivity changes (i.e., changes in relative retention) have been related to liquid crystalline stationary phases used in GC.<sup>86</sup>

Stationary phase properties can be varied over a wide range by selection of different polymerization methods and silane functionality. Higher surface coverages are achievable with trifunctional silanes and/or surface polymerization (self-assembled monolayer) approaches. Increasing ligand density leads to higher alkyl chain order and to diminished sorption of polar solvent, hence to decreased polarity and enhanced polarizability of the interphase. This, in turn, causes enhanced sorption of lipophilic solute molecules. In addition, the free volume between the alkyl chains decreases, resulting in reduced sorption of spherical molecules. It would appear that at high ligand densities (here >4.9  $\mu\text{mol}/\text{m}^2$ ), the kinetics of solute transfer between the stationary phase and the mobile phase are limited, perhaps due to stronger solute/stationary phase interactions, leading to strong tailing for these phases (column **D**).

A schematic illustration of the architecture (conformational alkyl chain order and chain spacing) of phases **A–D** is presented in Figure 12, summarizing the findings from solid-state NMR, fluorescence, and LC investigations. We have chosen TPM and DPH, two solutes with significantly different shape, as examples to illustrate molecular recognition processes. Motional freedom of DPH as revealed by fluorescence data is illustrated in Figure 12 for each of the four phases. It is also clear that phase thickness is strongly influenced by the presence and the amount of trans conformations. Material **A** (difunctional silane, solution polymerization) is characterized as follows. Its alkyl chains are flexible and disordered at room temperature, leading to reduced molecular shape recognition for rigid solutes. Fluorescence investigations reveal that DPH is fairly mobile within this type of stationary phase. Phase **B** (difunctional silane, surface polymerization) and phase **C** (trifunctional silane, solution polymerization) possess similar surface coverage; hence, they must differ in their architecture. NMR studies reveal that the alkyl chain arrangement is more ordered for material **C** at ambient temperatures. This leads to a reduced mobility of DPH between the immobilized alkyl chains and thus to greater shape selectivity. Given the similar bonding density, alkyl chain spacing must be wider (and more regular) for type **B** (surface polymerization).

It is useful to discuss the properties of material **D** in more detail. For conventional monomeric bonded phases, surface coverages are typically 3–4  $\mu\text{mol}/\text{m}^2$ , corresponding to reaction of 40–50% of the surface silanol groups (8.08  $\mu\text{mol}/\text{m}^2$  on silica gel).<sup>87</sup> The higher surface coverages of polymeric interphases are believed to result from high-density silane clusters or patches that result as a consequence of the polymerization chemistry.<sup>26</sup>

(86) Wise, S. A.; Sander, L. C.; Chang, H.; Markides, K. E.; Lee, M. L. *Chromatographia* **1988**, *25*, 473–480.

(87) Nyburg, S. C.; Lüth, H. *Acta Crystallogr.* **1972**, *B28*, 2992–2995.

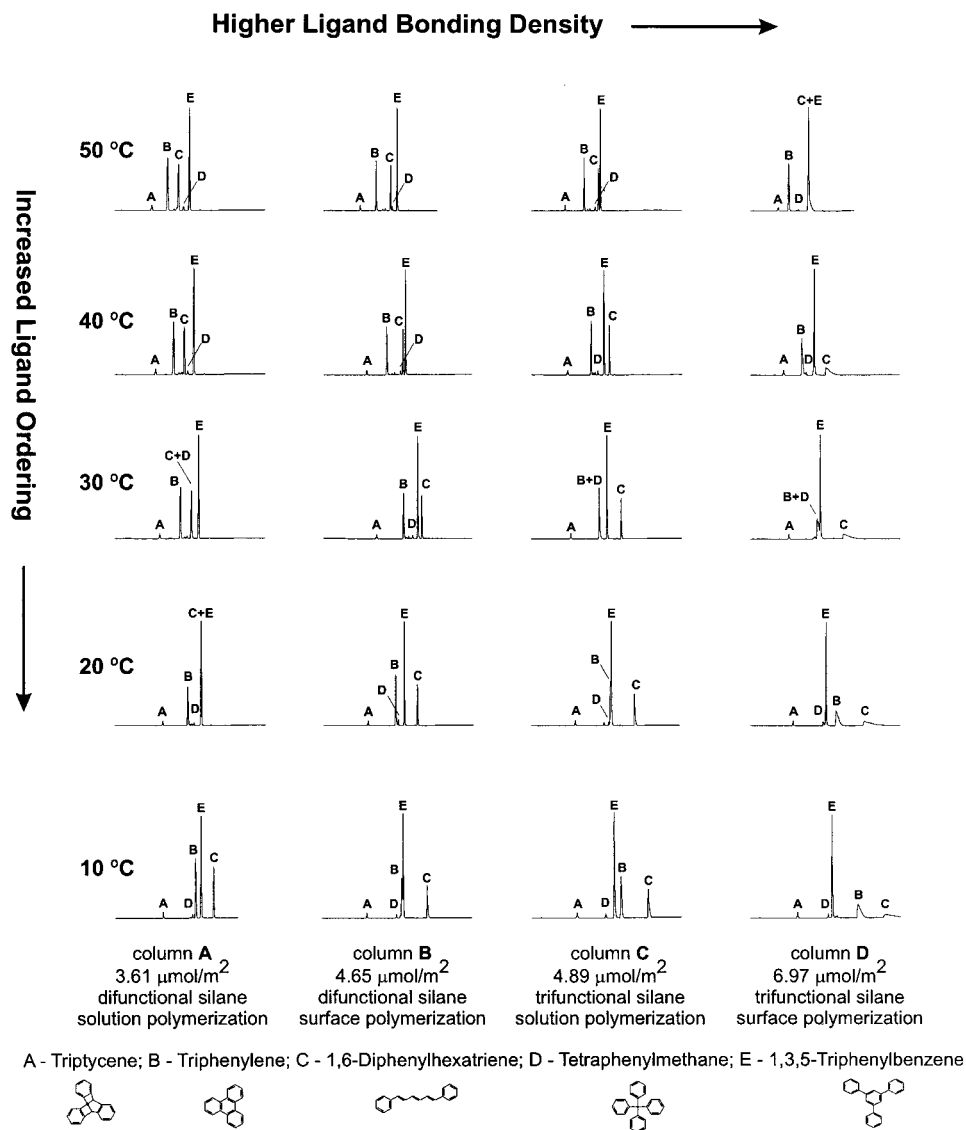


**Figure 11.** PAH separations of shape selectivity solutes at different temperatures.

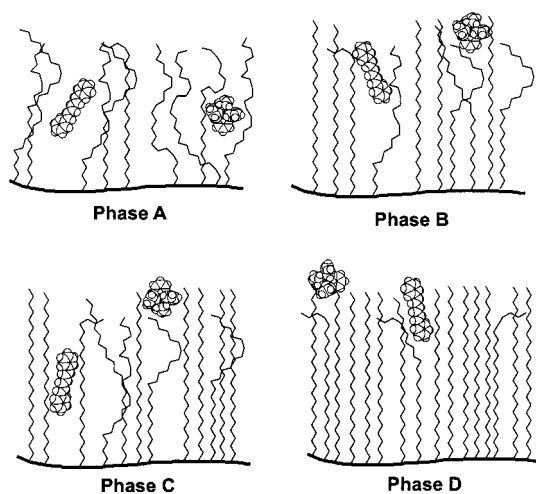


**Figure 12.** Schematic representation of the molecular recognition behavior of different  $\text{C}_{22}$  interphase types on the basis of solid-state NMR, fluorescence, and HPLC data.

The ligand density in polymeric phases is, in part, dictated by the Si—O—Si distance in the silane polymer, whereas for monomeric phases the steric hindrance of bound alkyl groups

is most responsible for the incomplete surface reaction. In the self-assembled monolayer strategy (surface polymerization), the reaction occurs with physisorbed water at the silica surface. Very high surface coverages should be achievable, and material **D** is likely to consist of almost a two-dimensional, crystalline  $\text{C}_{22}$  monolayer, as its surface coverage approaches  $\sim 90\%$  of the crystalline packing density ( $6.97$  vs  $8.08 \mu\text{mol}/\text{m}^2$ ).<sup>88</sup> This is consistent with the strong  $^{13}\text{C}$  NMR signal of trans conformations, the continued alkyl chain rigidity even at high temperatures, and the higher than expected wobble in cone angle determined by fluorescence spectroscopy. The high degree of order within the bonded phase also helps to explain the unique chromatographic selectivity for PAH solutes with different shapes.

(88) Urden, G.; Thoernwall, M.; Lyrenaes, S.; Lindstroem, L.; Nyberg, F. *Biomed. Chromatogr.* **1996**, *10*, 149–154.

(89) Wheeler, J. F.; Beck, T. L.; Klatte, S. J.; Cole, L. A.; Dorsey, J. G. *J. Chromatogr. A* **1993**, *656*, 317–333.

(90) Tchapla, A.; Heron, S.; Lesellier, E. *J. Chromatogr.* **1993**, *656*, 81–112.

(91) Certain commercial equipment, instruments, or materials are identified in this report to specify adequately the experimental procedure. Such identification does not imply recommendation or endorsement by the National Institute of Standards and Technology, nor does it imply that the materials or equipment identified are necessarily the best available for the purpose.

Assumptions on the dependence of chain order on bonding density and temperature as made by liquid chromatographic experiments<sup>89,90</sup> are supported here by complementary spectroscopic data. NMR and fluorescence investigations reveal that there is no sudden phase transition for alkyl chains, but that a gradual order/disorder process occurs with temperature.

### Conclusions

Solid-state NMR spectroscopy, fluorescence spectroscopy, and liquid chromatography have been used to study the architecture and molecular recognition behavior of various C<sub>22</sub> interphases. All investigation methods show that chain order increases with ligand density. The materials' properties differ considerably, from liquidlike, disordered alkyl chain arrangements (3.61  $\mu\text{mol}/\text{m}^2$ ) to a self-assembled monolayer phase with very high chain order (6.97  $\mu\text{mol}/\text{m}^2$ ). Penetration of DPH within the stationary phase was greatest in the solution-polymerized interphase (4.89  $\mu\text{mol}/\text{m}^2$ ). Solid-state NMR and fluorescence spectroscopies provide complementary data. Fluorescence spectroscopy permits the study of solutes within the bonded phase, and NMR spectroscopy gives detailed information on structure and mobility of the interphase itself. Indirect information on alkyl chain order is provided by LC separations of shape-selective solutes.

**Acknowledgment.** This work was supported by the Deutsche Forschungsgemeinschaft (DFG, Forschergruppe, Grant No. Li 154/41-3). M.P. would like to thank the Deutscher Akademischer Austauschdienst (DAAD) and the Alexander von Humboldt Foundation for providing support for research visits at NIST. The authors thank S. Strohschein (Institut für Organische Chemie) for performing LC–NMR experiments and YMC Inc. (R. Cooley) and YMC Europe GmbH (A. Kupka) for donations of silica gel. We thank J. R. Lakowicz (University of Maryland, School of Medicine, Baltimore, MD) for providing access to the Center of Fluorescence Spectroscopy and H. Malak (University of Maryland) for technical support and helpful discussions. David L. Vanderhart (NIST) is acknowledged for his comments concerning the manuscript.

**Supporting Information Available:** 2D WISE NMR spectra of phases **A** and **D** at 295 K, fluorescence anisotropy decay curves of DPH in suspensions of phase **C** at different solvent compositions, and tables listing photophysical data of DPH in suspensions of four different C<sub>22</sub> phases and of phase **C** in solvent mixtures of different water content (PDF). This material is available free of charge via the Internet at <http://pubs.acs.org>.

JA983046P